Available online at www.easdprocedia.org
EASD Procedia EURODYN (2020) 2244-2259

EASD
Procedia

EURODYN 2020
XI International Conference on Structural Dynamics
M. Papadrakakis, M. Fragiadakis, C. Papadimitriou (eds.)
Athens, Greece, 23–26 November 2020

STATISTICAL PROCESS CONTROL PROCEDURES FOR ONLINE DAMAGE DETECTION OF A MONUMENTAL MASONRY PALACE: THE CONSOLI PALACE IN GUBBIO, ITALY

Enrique García-Macías[1] and Filippo Ubertini[2]

[1]Department of Civil and Environmental Engineering, University of Perugia
Via G Duranti 93, Perugia 06125, Italy
enrique.garciamacias@unipg.it

[2] Department of Civil and Environmental Engineering, University of Perugia
Via G Duranti 93, Perugia 06125, Italy
filippo.ubertini@unipg.it

Keywords: Damage identification, Historic buildings, Structural health monitoring, Automated modal identification, Control chart, Machine Learning.

Abstract. *This paper proposes a new semi-supervised two-class pattern classification method for early damage detection of structures. The proposed approach comprises five consecutive steps, including the (i) collection of data samples representing the healthy condition of the structure (training period); (ii) clustering analysis; (iii) outliers elimination; (iv) pattern recognition using local Principal Components Analysis; and (v) pattern classification through control charts. The effectiveness of the proposed approach is demonstrated through two different case studies. These include a benchmark beam simulation model, and the Consoli Palace in Gubbio (Italy). The latter has been monitored for two years using a long-term vibration-based monitoring system, and represents an extraordinary example of a stiff masonry building with complex environmental effects. Analyses and discussion are presented covering the effects of differing structural/environmental behaviour regimes, the presence of outliers in the training period, and the effectiveness of different control charts.*

doi: 10.47964/1120.9181.18809

1 INTRODUCTION

The heightened awareness about the importance of the conservation of heritage structures has fostered the implementation of numerous Structural Health Monitoring (SHM) systems in recent years [14, 9, 5, 10]. In particular, ambient vibration-based SHM systems are becoming particularly popular owing to their capability of performing a non-destructive assessment of the structural integrity with minimum architectural impact and without affecting the normal operating conditions of structures [2, 4, 15]. Through Automated Operational Modal Analysis (A-OMA) techniques, such systems allow the tracking of the modal features of structures and, in turn, it is possible to detect damage-induced anomalies and so enable the decision-making of condition-based rehabilitation [17, 18]. Nevertheless, the development of efficient SHM methodologies for early damage detection still remains an open and active research area.

Specifically, the SHM of masonry structures is specially challenging due to the complex dependence of their intrinsic stiffness on environmental factors (mainly temperature and humidity), often resulting in different behaviour regimes [7, 5, 10]. This is the case, for instance, of masonry structures experiencing freezing conditions during the winter, when the icing of pore water in masonry leads to a dramatic change in temperature/stiffness relationship. Such environmental effects induce both daily and seasonal fluctuations in the modal features of structures, which usually mask damage-induced anomalies. In this regard, the application of advanced statistical process control procedures becomes imperative for early damage detection [3].

In this line, this paper presents a new semi-supervised two-class pattern classification method for early damage detection of structures. The proposed approach comprises five consecutive steps, including the (i) collection of data samples representing the healthy condition of the structure (training period); (ii) clustering analysis; (iii) outliers elimination; (iv) pattern recognition using local Principal Components Analysis; and (v) pattern classification using control charts. The effectiveness of the proposed approach is evaluated through two different case studies. These include a benchmark beam structure model, and the monumental Consoli Palace in Gubbio (Italy). The palace has been continuously monitored since July 2017 with a low-cost mixed static/dynamic/environmental long-term monitoring system [10]. In this work, the monitoring data of three high-sensitivity accelerometers and two thermocouples recording ambient vibrations and environmental temperatures are exploited. On this basis, the resonant frequencies of the palace have been identified and tracked using an A-OMA technique based upon the Covariance-based Stochastic Subspace Identification method (COV-SSI). The experimentally identified resonant frequencies are selected as damage-sensitive features, and the effectiveness of the proposed damage detection approach is evaluated considering artificial damage in the shape of frequency decays. The Consoli Palace represents an exceptional example of a stiff masonry building. Due to the low excitation levels in the building, the identified resonant frequencies present an elevated number of outliers that hinder the damage detection tasks. Additionally, the complex geometry of the palace and its connection with the adjoining buildings originates the existence of highly non-linear environmental effects, making it an outstanding benchmark structure for testing the proposed damage detection approach.

2 TWO-CLASS PATTERN CLASSIFICATION METHOD FOR DAMAGE DETECTION

This paper proposes a five step pattern classification algorithm for two-class damage detection as sketched in Fig. 1. The proposed approach comprises: (I) Characterization of the healthy condition of the structure with an initial training period; (II) Clustering analysis to identify the

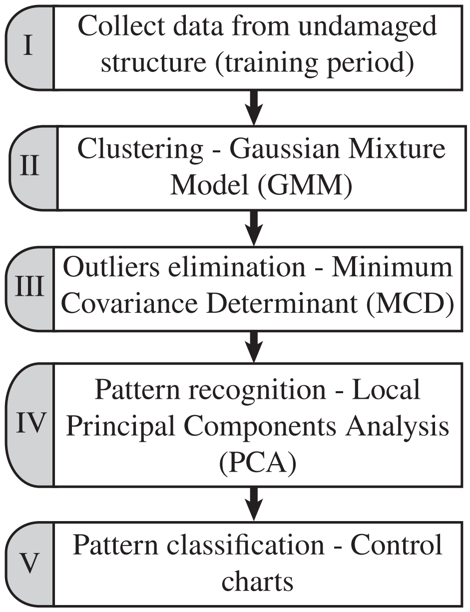

Figure 1: Flow chart of proposed two-class pattern classification algorithm for damage detection.

presence of multiple environmental regimes; (III) Outliers elimination; (IV) Pattern recognition through local PCA; and (V) Patter classification using control charts.

Let us consider that the SHM system performs an automated identification of m resonant frequencies f_i, $i = 1, \ldots, m$ as damage sensitive features. For notational convenience, let us denote the features at an instant n in vector form as $\mathbf{x}_n = \left[f_{(1,n)}, \ldots, f_{(m,n)}\right]$. We assume that the SHM system identifies a total of N sets of modal features, so the observation matrix $\mathbf{Y} \in \mathbb{R}^{N \times m}$ is constructed by collecting the features vectors by rows. In order to statistically characterize the healthy condition of the structure, a subset of tp data samples are selected as the training period. This must be long enough to cover the full range of environmental conditions (both daily and seasonal fluctuations), and typically a one-year period is assumed adequate. Note that the observation matrix $\mathbf{Y}$ represents a multivariate data set which, in principle, is composed of non-linear data.

2.1 CLUSTERING - GAUSSIAN MIXTURE MODEL

In order to take into account different environmental mechanisms, the damage sensitive features in the training period are clustered into different data sets using a GMM model. This approach assumes that the probability density function $p(\mathbf{x})$ of the data set in the training period $\mathbf{X}$ (in general, non-normally distributed) can be represented as a linear superposition of K Gaussian components as [1]:

$$p(\mathbf{x}) = \sum_{k=1}^{K} \pi_k \mathcal{N}\left(\mathbf{x} \,|\, \boldsymbol{\mu}_k, \boldsymbol{\Sigma}_k\right). \tag{1}$$

Each component of the mixture is defined as a Gaussian distribution $\mathcal{N}\left(\mathbf{x} \,|\, \boldsymbol{\mu}_k, \boldsymbol{\Sigma}_k\right)$ with mean and covariance matrix denoted by $\boldsymbol{\mu}_k$ and $\boldsymbol{\Sigma}_k$, respectively. The parameters $\boldsymbol{\pi} = [\pi_1, \ldots, \pi_K]^{\mathrm{T}}$ in Eq. (1) are called the mixing coefficients, and they range between 0 and 1 ($0 \leq \pi_k \leq 1$) and sum to one ($\sum_{k=1}^{K} \pi_k = 1$). The model parameters, $\boldsymbol{\mu}_k$,$\boldsymbol{\Sigma}_k$ and π_k, are fitted by minimizing the log-likelihood function:

$$\ln p(\mathbf{X}\,|\boldsymbol{\pi},\boldsymbol{\mu},\boldsymbol{\Sigma}\,) = \sum_{n=1}^{t_p} \ln\left\{\sum_{k=1}^{K} \pi_k \mathcal{N}\left(\mathbf{x}_n\,|\boldsymbol{\mu}_k,\boldsymbol{\Sigma}_k\,\right)\right\}. \tag{2}$$

The maximum likelihood solution for the parameters ($\boldsymbol{\mu}$,$\boldsymbol{\Sigma}$ and $\boldsymbol{\pi}$) is estimated using the iterative Expectation-Maximization (EM) algorithm. In the expectation (E) step, the parameters (initial guess at the beginning) are held fixed and the posterior probability of assigning $\mathbf{x}_n$ to the k's cluster is given by the so-called responsibilities $\gamma(z_{nk})$ as:

$$\gamma(z_{nk}) = \frac{\pi_k \mathcal{N}\left(\mathbf{x}_n\,|\boldsymbol{\mu}_k,\boldsymbol{\Sigma}_k\,\right)}{\sum_{j=1}^{K} \pi_j \mathcal{N}\left(\mathbf{x}_n\,|\boldsymbol{\mu}_j,\boldsymbol{\Sigma}_j\,\right)}, \tag{3}$$

where z_{nk} is an element of a K-dimensional binary random variable **z** with a 1-of-K representation. Only one element in **z** is equal to 1 and all other elements are 0.

Then, in the maximization (M) step, the parameters are re-estimated using the posterior probability calculated in the previous E step as follows:

$$\boldsymbol{\mu}_k^{new} = \frac{1}{N_k}\sum_{n=1}^{t_p} \gamma(z_{nk})\mathbf{x}_n, \tag{4}$$

$$\boldsymbol{\Sigma}_k^{new} = \frac{1}{N_k}\sum_{n=1}^{t_p} \gamma(z_{nk})\left(\mathbf{x}_n - \boldsymbol{\mu}_k^{new}\right)\left(\mathbf{x}_n - \boldsymbol{\mu}_k^{new}\right)^{\mathrm{T}}, \tag{5}$$

$$\pi_k^{new} = N_k/N, \quad N_k = \sum_{n=1}^{t_p} \gamma(z_{nk}). \tag{6}$$

The log-likelihood in Eq. (2) can then be evaluated. Convergence of either the parameters of the log likelihood is checked, and if the criteria are not satisfied, the process is iterated using the updated data values until the criteria are met. Once the K clusters have been defined in the training period, new data samples are assigned to the cluster with the least Mahalanobis distance.

2.2 OUTLIERS ELIMINATION

The Minimum Covariance Determinant (MCD) method [8] is used to minimize the effect of outlier measurements in the training population. The MCD method seeks a sample subset within a multivariate dataset that minimizes the covariance matrix. Specifically, the MCD method is applied in this work to every cluster identified in the training period. Consider an arbitrary cluster $\mathbf{C} = \{\mathbf{x}_1,\ldots,\mathbf{x}_d\}$ containing d samples, and let $H_1 \subset \{1,\ldots,d\}$ be an h-subset, that is $|H_1| = h$. Being $\boldsymbol{\mu}_1$ and $\boldsymbol{\Sigma}_1$ the empirical mean and covariance matrix of the data in H_1, the Mahalobis distances of all the data samples in the cluster read (det($\boldsymbol{\Sigma}_1$) $\neq 0$):

$$d_1(i) = \sqrt{\left(\mathbf{x}_i - \boldsymbol{\mu}_1\right)^{\mathrm{T}} \boldsymbol{\Sigma}_1^{-1}\left(\mathbf{x}_i - \boldsymbol{\mu}_1\right)} \quad \text{for} \quad i = 1,\ldots,d. \tag{7}$$

Now take H_2 another h-subset such that $\{d_1(i); i \in H_2\} := \{(d_1)_{1:d},\ldots,(d_1)_{h:d}\}$ where $(d_1)_{1:d} \leq (d_1)_{2:d} \leq \ldots \leq (d_1)_{d:d}$ are the ordered distances, and compute $\boldsymbol{\mu}_2$ and $\boldsymbol{\Sigma}_2$ based on H_2. Then det($\boldsymbol{\Sigma}_2$) $\leq$det($\boldsymbol{\Sigma}_1$) with equality if and only if $\boldsymbol{\mu}_2 = \boldsymbol{\mu}_1$ and $\boldsymbol{\Sigma}_2 = \boldsymbol{\Sigma}_1$. This process, also known as C-step, can be iteratively repeated. If det($\boldsymbol{\Sigma}_2$) $= 0$ or det($\boldsymbol{\Sigma}_2$) $=$det($\boldsymbol{\Sigma}_1$), the algorithm stops; otherwise, another C-step is run yielding $\det(\mathbf{\Sigma}_3)$, and so on. The sequence $\det(\mathbf{\Sigma}_1) \geq \det(\mathbf{\Sigma}_2) \geq \det(\mathbf{\Sigma}_3) \geq \ldots$ is nonnegative and hence must converge, so there must be an index s such that $\det(\mathbf{\Sigma}_s) = 0$ or $\det(\mathbf{\Sigma}_s) = \det(\mathbf{\Sigma}_{s-1})$. In this work, the fast implementation of the MCD method proposed by Rousseeuw and Driessen [16] has been implemented. The dimension h of the subsets has been selected as $0.8d$. Once the algorithm converges, a certain percentage of the samples with the largest Mahalanobis distances with respect to the converged sample subset are considered as outliers and eliminated.

2.3 PRINCIPAL COMPONENTS ANALYSIS

Once the detected outliers have been eliminated from the clusters, pattern recognition using PCA is conducted for every cluster in the training period. Principal Component Analysis consists of a double change of coordinates, where the original data are first projected in the vectorial space generated by the principal components (PCs) and then remapped back to the original space by retaining only some of the PCs. Let us denote the matrix of observations $\mathbf{X}_{c_k} \in \mathbb{R}^{n_{c_k} \times m}$ in an arbitrary cluster c_k $(k = 1, \ldots, K)$ of size n_{c_k} and $\mathbf{X}^*_{c_k} \in \mathbb{R}^{n_{c_k} \times m}$ a matrix whose columns are the centred variables $\mathbf{x}^*_j$ (i.e. $x^*_{ij} = x_{ij} - \overline{x}_j$, where $\overline{x}_j$ denotes the mean value of the observations on variable j). Then, the eigendecomposition of the covariance matrix $\mathbf{\Sigma}$ reads:

$$\mathbf{\Sigma} = \left(\mathbf{X}^*_{c_k}\right)^{\mathrm{T}} \mathbf{X}^*_{c_k} = \mathbf{U}_{c_k} \mathbf{S}^2 \mathbf{U}^{\mathrm{T}}_{c_k}, \tag{8}$$

where $\mathbf{U}_{c_k} \in \mathbb{R}^{n_{c_k} \times n_{c_k}}$ is the so-called loading matrix. The eigenvalues of the covariance matrix contained in the diagonal matrix $\mathbf{S}^2$ represent the variance contributions of each PC. Assuming that the PCs providing the largest contributions to the variance represent the effects of environmental and operational factors, it is possible to find an approximation $\widehat{\mathbf{X}}^*_{c_k}$ isolating such factors through dimensionality reduction. This can be done by retaining only the first l columns of matrix $\mathbf{U}_{c_k}$ in Eq. (8) into a rectangular reduced loading matrix, $\widehat{\mathbf{U}}_{c_k} \in \mathbb{R}^{l \times m}$. Hence, matrix $\widehat{\mathbf{X}}^*_{c_k}$ is estimated as:

$$\widehat{\mathbf{X}}^*_{c_k} = \mathbf{X}^*_{c_k} \widehat{\mathbf{U}}_{c_k} \widehat{\mathbf{U}}^{\mathrm{T}}_{c_k}, \tag{9}$$

which represents the backward transformation of the original observations in $\mathbf{X}^*_{c_k}$ from a reduced space of the l PCs to the original one. Since the transformation in Eq. (9) provides a representation of the environmental/operational effects, matrix $\widehat{\mathbf{U}}_{c_k}$ allows to predict the resonant frequencies of the structure beyond the training period.

2.4 CONTROL CHARTS

Once the transformation matrices $\widehat{\mathbf{U}}_{c_k}$ are obtained for all the identified clusters c_k $(k = 1, \ldots, K)$ in the training period, it is possible to compute a matrix of predicted resonant frequencies $\widehat{\mathbf{Y}} \in \mathbb{R}^{N \times m}$ throughout all the monitoring period. Since the statistical models used to construct $\widehat{\mathbf{Y}}$ are fitted using the training period representing a baseline in-control population where the structure is assumed to remain healthy, the appearance of damage can be inferred from the detection of anomalies in the residual error matrix $\mathbf{E} \in \mathbb{R}^{N \times m}$ computed as:

$$\mathbf{E} = \mathbf{Y} - \widehat{\mathbf{Y}}. \tag{10}$$

Assuming that $\widehat{\mathbf{Y}}$ reproduces the part of the variance in the resonant frequencies related to environmental/operational changes, $\mathbf{E}$ only contains the residual variance stemming from identification errors, un-modelled environmental/operational effects, and structural defects. Therefore, the presence of damage in the shape of anomalies in the time series of $\mathbf{E}$ can be revealed through control charts. These furnish time series of certain statistical distances between the distribution of the residuals contained in $\mathbf{E}$ and the in-control data base. Specifically, two different control charts are used in this work, including the Hotelling (T^2) and Multivariate Exponentially Weighted Moving Average (MEWMA) control charts. The statistical distances handled by these control charts are positive by definition, so an in-control region can be specified by an interval [0,*UCL*]. The upper control limit (*UCL*) can be estimated as the statistical distance attaining a certain confidence (exceeding) level α in the training database. In this light, the appearance of out-of-control processes violating the in-control region may indicate the appearance of damage.

- *Hotelling's* T^2: The Hotelling's T^2 control chart [6] is defined as:

$$T_i^2 = r\left(\overline{\mathbf{E}} - \overline{\overline{\mathbf{E}}}\right)^{\mathrm{T}} \mathbf{\Sigma}_0^{-1} \left(\overline{\mathbf{E}} - \overline{\overline{\mathbf{E}}}\right),\ i = 1, 2, \ldots, N/r, \tag{11}$$

  where r is an integer parameter referred to as subgroup size, $\overline{\mathbf{E}}$ is the mean of the residuals in the subgroup of the last r observations, while $\overline{\overline{\mathbf{E}}}$ and $\mathbf{\Sigma}_0$ are the mean values and the covariance matrix of the residuals statistically estimated in the training period.

- *Multivariate Exponentially Weighted Moving Average (MEWMA)*: Originally proposed by Lowry *et al*. [12], the MEWMA control chart represents an intermediate solution between the T^2 and the MCUSUM control charts. Alike the MCUSUM control chart, the MEWMA method also accounts for the information from past observations, although it gives weights decreasing in a geometric progression from the most recent observation to the first one. The statistical distance used in the MEWMA control chart reads:

$$MEWMA_i = \left(r\,\mathbf{z}_i^{\mathrm{T}} \mathbf{\Sigma}_{z_i}^{-1} \mathbf{z}_i\right)^{1/2},\ i = 1, 2, \ldots, N/r, \tag{12}$$

  with

$$\begin{aligned} \mathbf{z}_i &= \lambda\left(\overline{\mathbf{E}} - \overline{\overline{\mathbf{E}}}\right) + (1-\lambda)\mathbf{z}_{i-1}, \\ \mathbf{\Sigma}_{z_i} &= \lambda \frac{1-(1-\lambda)^{2i}}{2-\lambda} \mathbf{\Sigma}_0, \end{aligned} \tag{13}$$

  where λ is a smoothing constant with $0 \leq \lambda \leq 1$. Practically, the most often used value of λ is 0.1.

3 CASE STUDIES

To illustrate the capabilities of the proposed approach for early-damage detection, two case studies are examined in this section. The first one is a numerical beam model which is subjected to changing temperature conditions and varying mass distribution. The second one is a real-life case study, the Consoli Palace in Gubbio (Italy), which was monitored for almost two years.

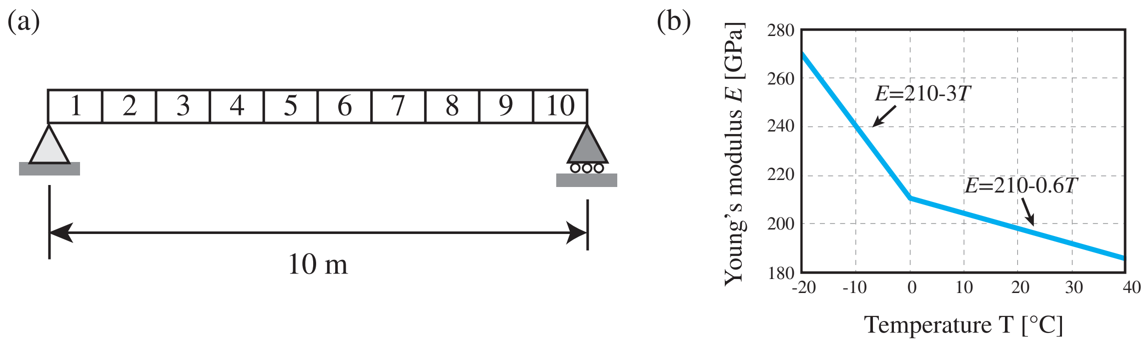

Figure 2: Beam structure model (a) and variations of Young's modulus with temperature for the beam structure model (b).

3.1 Beam structure model

The first case study is the benchmark beam model previously reported in references [11, 20] and sketched in Fig. 2 (a). The model consists of a 10 m long simply supported beam defined by ten 2-nodes beam-bending elements of 1 m each. The beam has constant cross-section, inertia and mass density of 0.08 m^2, 0.0006 m^4, and 7850 kg/m^3, respectively. The Young's modulus of the beam is assumed to be temperature dependent according to the bi-linear relationship shown in Fig. 2 (b).

The first four natural frequencies of the beam are used as damage sensitive features. In particular, seven consecutive set ups are analysed as summarised in Table 1. The training period is defined by the first two data sets (UC-1 and UC-2). The first one includes 800 and 420 observations with temperatures between 0°C and 40°C and between -20°C and 0°C, respectively. In addition, a random variation of $\pm 10\%$ in the mass density of the beam is also considered in order to include some randomness in the observations. The second data set has 400 observations for temperatures between 0°C and 40°C and 210 between -20°C and 0°C. In this case, a larger variation in density of $\pm 25\%$ is considered as a way of simulating the presence of outlier measurements. Afterwards, five damage cases with increasing severities (25%, 30%, 35%, 40% and 45%), labelled from DC-1 to DC-5 in Table 1, are considered. Specifically, damages are simulated through reductions in the bending stiffness of the 4th element. Data from each damaged case are obtained considering 200 samples with temperatures ranging between 0°C and 40°C, and 100 samples between -20°C and 0°C. Moreover, each element is assumed to have a $\pm 10\%$ random variation in density.

	UC-1		UC-2		DC-1		DC-2		DC-3		DC-4		DC-5	
Samples	800	420	400	210	200	100	200	100	200	100	200	100	200	100
ΔT^a	T_1	T_2	T_1	T_2	T_1	T_2	T_1	T_2	T_1	T_2	T_1	T_2	T_1	T_2
$\Delta\rho^b$ [$\pm$%]	10	10	25	25	10	10	10	10	10	10	10	10	10	10
Damage^c [%]	0	0	0	0	25	25	30	30	35	35	40	40	45	45

^{a} T_1: [0°C,40°C], T_2: [-20°C,0°C].
^{b} $\Delta\rho$ *denotes the relative variation of the mass density of the beam.*
^{c} *Damage severity defined as a reduction of the bending stiffness of the 4th element.*

Table 1: Data samples considered in the beam structure model.

Figure 3 depicts the plots of environmental temperature versus the four natural frequencies

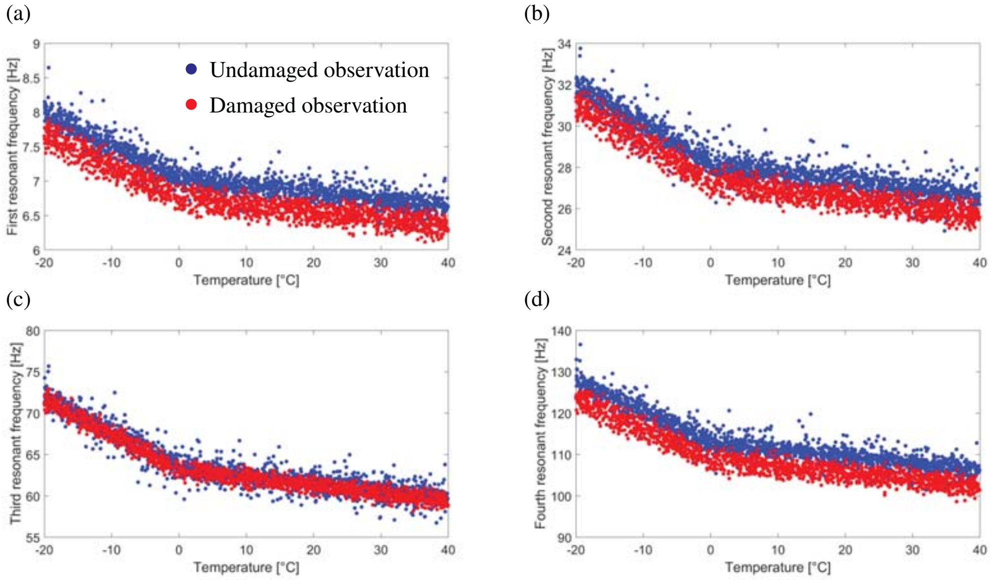

Figure 3: Plot of temperature versus (a) first natural frequency, (b) second natural frequency, (c) third natural frequency and (d) fourth natural frequency of the beam structure model.

of beam structure model. It is interesting to note that the damaged and undamaged observations intermix and can be hardly distinguished from one another in the third resonant frequency. The third mode is relatively insensitive to the presence of damage since the fourth element is located near a node of this mode. In the rest of the modes, some of the damaged observations cluster together with the undamaged cases, specially in the space containing the outlier measurements. Therefore, these outliers need to be identified and removed from the database before applying damage detection methods. To do so, the proposed approach sketched in Fig. 1 is applied herein. Firstly, the GMM model is applied to differentiate the two different environmental regimes in the time series of resonant frequencies. The result, shown in Fig. 4, shows that the GMM model can accurately separate between resonant frequencies obtained with temperatures ranging between -20°C and 0°C (Cold observations) and between 0°C and 40°C (Hot observations). Afterwards, the outliers detection algorithm previously overviewed in Section 2.2 can be applied independently to each cluster. In particular, a percentage of 30% of the data samples with the largest Mahalanobis distances according to Eq. (7) are considered as outliers. The result of the outliers elimination algorithm applied to the training period (UC-1 and UC-2) is shown in Fig. 5. It can be seen that most of the detected outliers surround the clean measurements.

Then, a PCA model can be fitted using the clean training database. In this case, one single PC sufficed to explain more than 95% of the variance of the resonant frequencies in the two clusters. The comparison between the predictions of the resonant frequencies by the PCA model and the numerical ones is presented in Fig. 6. The low scatter of the points around the diagonal line corroborates that the PCA model is formed with accuracy. This model can now be used to detect the appearance of damage beyond the training period according to the approach previously presented in Section 2.3. Specifically, Fig. 7 shows the Hotelling's control charts obtained without applying (a) and applying (b) the outliers elimination algorithm. The effect of the presence of outliers in the training period is clearly exemplified in Fig. 7 (a). In this graph, the presence of outliers between the observation numbers 1020 and 1830 lead to a large UCL (confidence level 95%) and corrupts the estimation of the mean vector $\overline{\overline{\mathbf{E}}}$ and covariance matrix

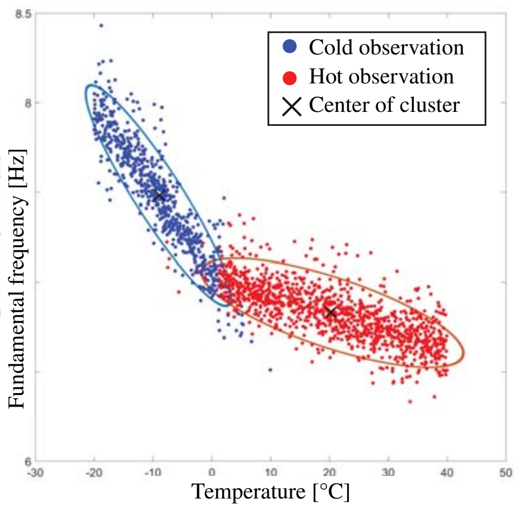

Figure 4: Cluster of the first resonant frequency with temperature of the beam structure model using GMM.

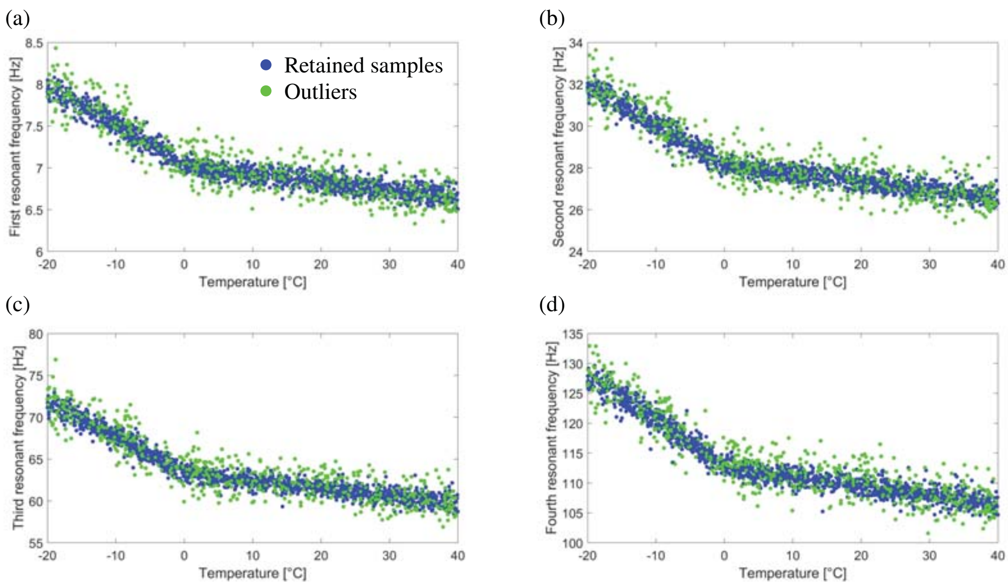

Figure 5: Plot of temperature versus (a) first natural frequency, (b) second natural frequency, (c) third natural frequency and (d) fourth natural frequency of clean undamaged observations, outlier undamaged observations and damaged observations of the beam structure model.

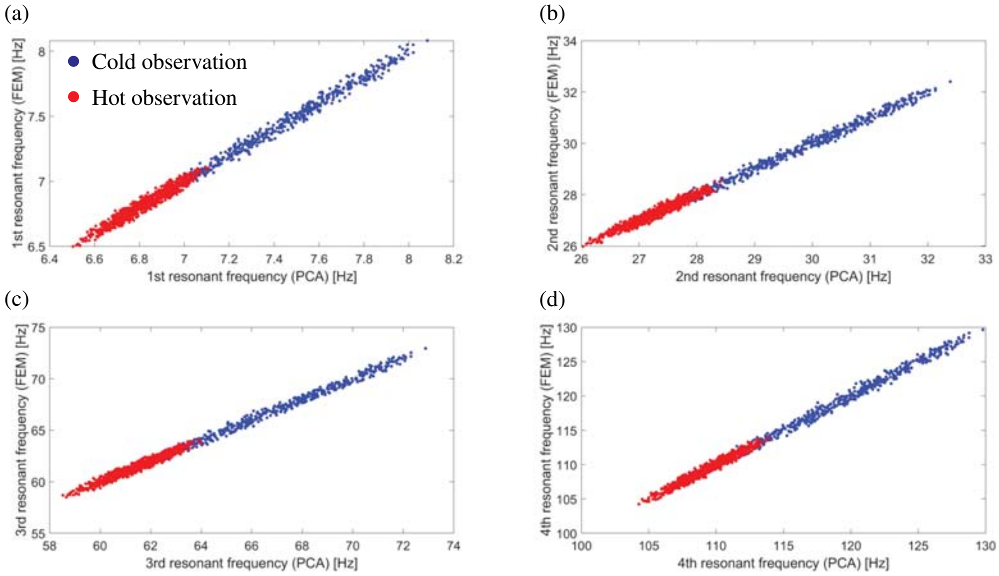

Figure 6: Plot of numerical estimates and predictions of the PCA model in terms of the (a) first natural frequency, (b) second natural frequency, (c) third natural frequency and (d) fourth natural frequency of the beam structure model ($r = 1$)

of the residuals $\mathbf{\Sigma}_0$ in the training period. This hinders the detection of mild damage severities, not being possible the identification until the damage severity of 35%-40%. Conversely, the control chart in 7 (b) shows that the outliers elimination algorithm effectively eliminates most of the outliers in the observation numbers between 1020 and 1830. This leads to a considerably smaller UCL and better estimation of $\overline{\overline{\mathbf{E}}}$ and $\mathbf{\Sigma}_0$. This allows to accurately detect all the damaged cases.

3.2 Consoli Palace

The Consoli Palace (Fig. 8 (a)), located in the city of Gubbio in Italy, was erected between 1332 and 1349 and currently hosts the Civic Museum of Gubbio. The palace is 60 m high, including a bell-tower and a panoramic loggia, and has a rectangular plan of about 40×20 m. Within the framework of the Horizon 2020 European HERACLES project (2016-2018, heracles-project.eu), a permanent SHM system has been installed in the Consoli Palace since July 2017. Specifically, three PCB 393B12 accelerometers (A1, A2 and A3) were deployed on the roof level of the palace, as well as two K-type thermocouples to monitor the environmental temperature. The sensors are connected to a NI CompactDAQ-9132 data acquisition system with NI 9234 and NI 9219 acquisition modules for accelerations and temperatures, respectively. Ambient accelerations and temperatures were respectively sampled at 100 Hz and 0.1 Hz and stored in consecutive separate files containing 30 min-long recordings. The data files were sent online through the Internet to a remove server, where an in-house code for the management of integrated SHM systems called MOSS was used for automated SHM of the palace.

Figure 9 shows the time series of identified resonant frequencies using an automated version of the SSI-COV. Specifically, five modes corresponding to Fx1 (first global bending mode in the $x-$direction), Fy1 (first global bending mode in the $y-$direction), L1 (first order local mode related to the interaction between the palace and the bell-tower), T1 (global torsional mode), and L3 (third order local mode) were tracked in the Consoli Palace. For more specific information on the adopted A-OMA technique and identification results of the Consoli Palace, readers may

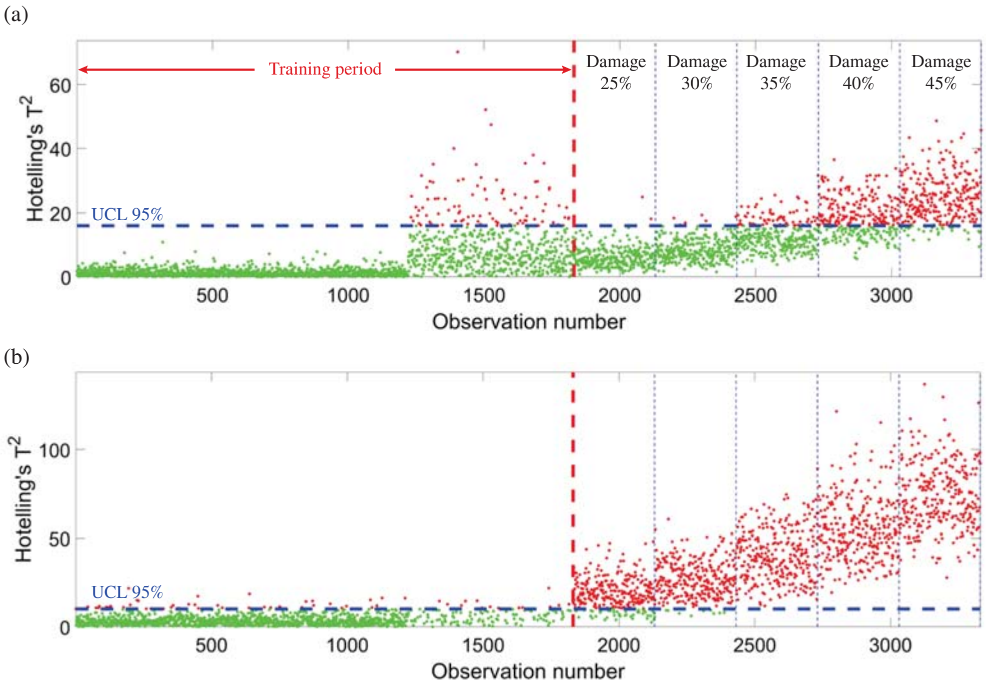

Figure 7: Comparison between the Hotelling's control charts obtained without applying (a) and applying the outliers elimination algorithm (b).

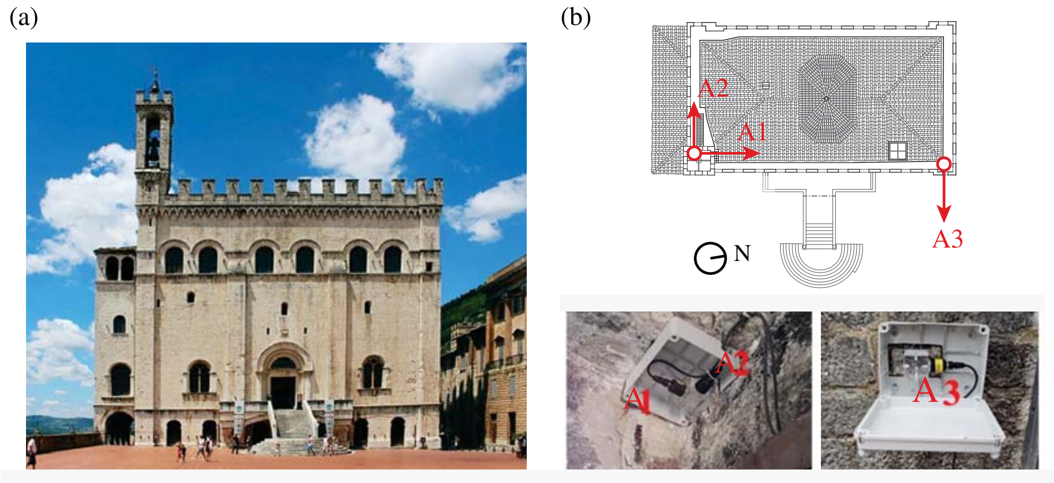

Figure 8: View of the Consoli Palace (a), and sketch of the monitoring system (b).

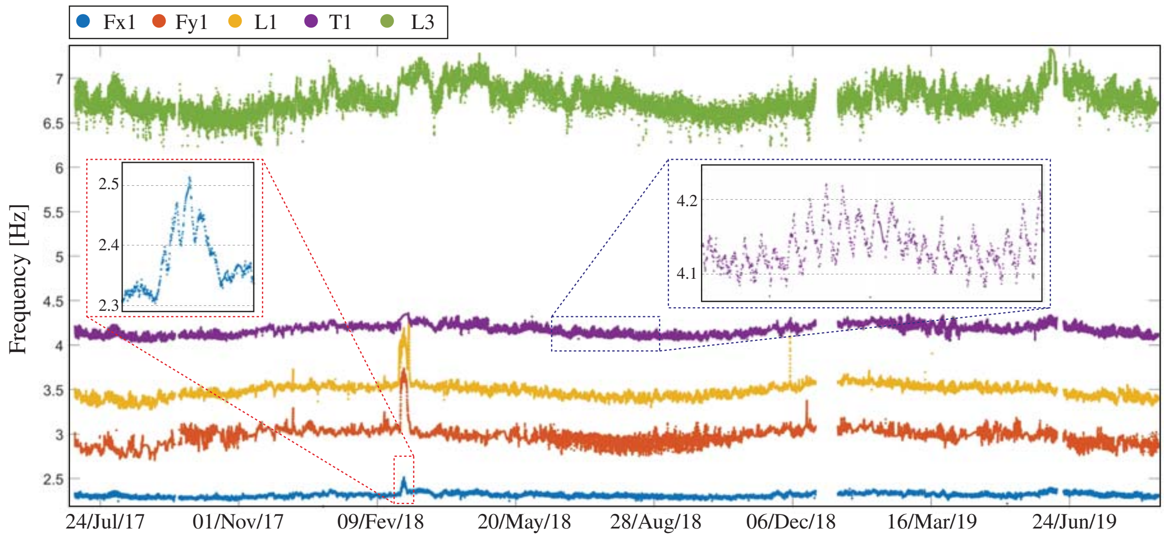

Figure 9: Frequency tracking results of the permanent SHM system installed in the Consoli Palace.

refer to references [13, 19, 10]. It is interesting to note that local sudden increases in the resonant frequencies were found during the time period from February 25$^{\text{th}}$ to March 1$^{\text{st}}$ 2017. Freezing air temperatures were registered during these days, thereby such increases are conceivably due to the formation of ice in the micro porosity of the mortar joints and the consequent stiffening effect.

Figure 10 plots the fundamental frequency versus environmental temperature throughout the training period of one year. In this figure, the presence of freezing conditions is evident in the shape of hasty frequency increases. Moreover, it is noted that the frequency-temperature relationship is not linear, but describes a non-linear behaviour with certain hysteresis. Such a behaviour may be due to the intricate geometry and distribution of volumes of the palace, which presumably originate the presence of complex temperature/humidity gradients throughout the building. In this case, the use of clustering approaches for the discrimination of different environmental regimes becomes imperatives. Specifically, two different GMM models have been investigated, one using 5 clusters in Fig. 10 (a) and a second one only using 2 clusters in Fig. 10 (b). It is noted that the database corresponding to the frequencies under freezing conditions is well captured by both modes. Additionally, it is interesting to note that the GMM model with the largest number of clusters differentiate four clusters in the frequency-temperature hysteresis cycles. Two clusters (cyan and blue) collect the data samples with minimum/maximum temperature values, while two other clusters (green and red) separate the two branches closing the hysteresis cycles. This fact may indicate the existence of distinct cooling and heating mechanisms.

Once the tracked resonant frequencies have been classified into clusters, the outliers elimination algorithm is applied to the database of the training period. Specifically, a percentage of 5% of the data samples with the largest Mahalanobis distances have been eliminated. Additionally, since freezing conditions are only observed in a poorly populated cluster, all the samples corresponding to this cluster have been dismissed. The resulting clean training population has been used to construct the statistical models and so eliminate the effects of environmental factors. Specifically, the GMM model in Fig. 10 (a) has been used to build a four-member PCA model. In all the the sub-models, only 2 PCs have been retained since they sufficed to explain more than

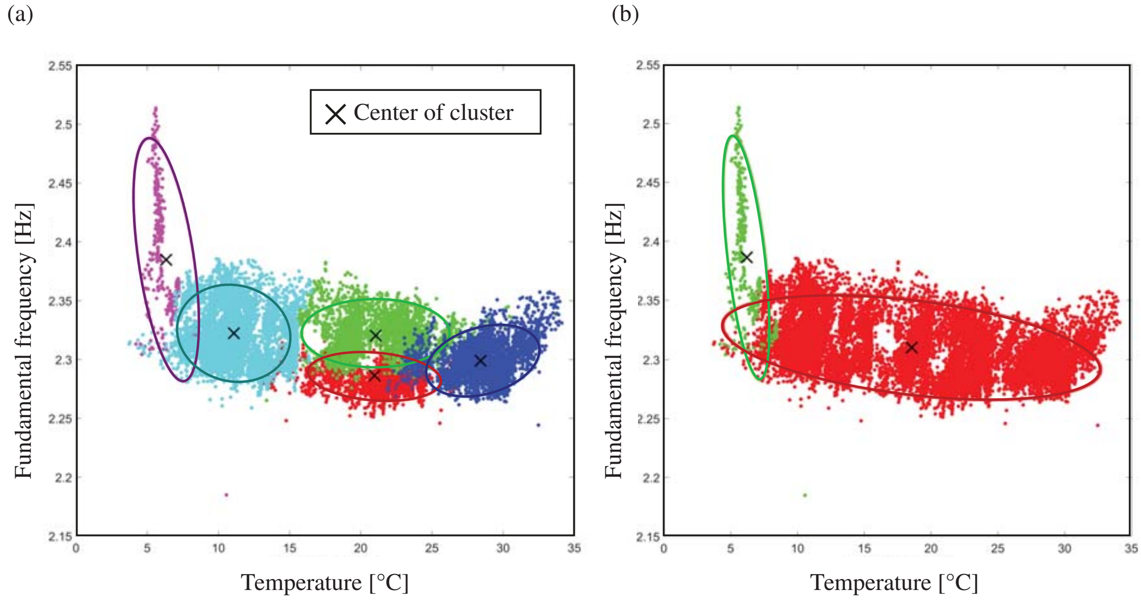

Figure 10: Clustering results of the resonant frequencies of the Consoli Palace using the GMM model considering five clusters (a) and two clusters (b).

95% of the variance of the resonant frequencies of the clusters. On the other hand, for comparison purposes, the GMM model in Fig. 10 (b) has been used to construct an AutoAssociative Neural Network (AANN) [3]. This model is also known as non-linear PCA, and its architecture consists of three hidden layers: mapping, bottleneck, and de-mapping. In this particular work, the mapping, bottleneck, and de-mapping layers have been defined with 5, 3, and 5 neurons, respectively. Hyperbolic tangent sigmoid transfer functions have been selected, and the AANN has been trained using the Levenberg-Marquardt back-propagation method. AANNs have been reported to outperform standard PCA models when dealing with non-linear correlations, so their ability to reproduce the non-linear behaviour observed in Fig. 10 is tested herein by considering the two-cluster GMM model in Fig. 10 (b).

Figures 11 and 12 present the control charts obtained using the PCA and the AANN models, respectively. In these figures, two different cases are analysed, namely the experimentally identified resonant frequencies (undamaged) and a test case including artificial damage. Specifically, the remaining monitoring time after the training period has been divided into three segments, and frequency decays have been applied to the fundamental frequency in the last two segments. The artificial frequency decays have been selected as 0.4% (mild) and 1% (moderate). Additionally, the results obtained using the Hotelling and the MEWMA control charts are also reported. It is noted in all the undamaged cases using the Hotelling's control chart that, although the UCL has been estimated for a confidence level of 95% (5% of outliers), the percentage of outliers is consistently greater than 10% beyond the training period. This fact may indicate limitations of the regression models, frequency tracking errors, or an insufficient training period. Moreover, it is also noticeable that the MEWMA control chart is more sensitive to shifts in the mean values of residuals. Let us focus first on the results obtained with the PCA model in Fig. 11. It is observed that the percentage of outliers in the damaged sections of the Hotelling's control chart goes from 10% and 15.6% (undamaged) to 16% ($\Delta Fx1 = -0.4\%$) and 41.3% ($\Delta Fx1 = -1.0\%$). That is to say, frequency decays of $\Delta Fx1 = -0.4\%$ and $\Delta Fx1 = -1.0\%$ lead to increases in the number of out-of-control samples of 16.0% and 164.74%, respectively. On the other hand, the number of outliers in the damaged sections of the MEWMA control chart

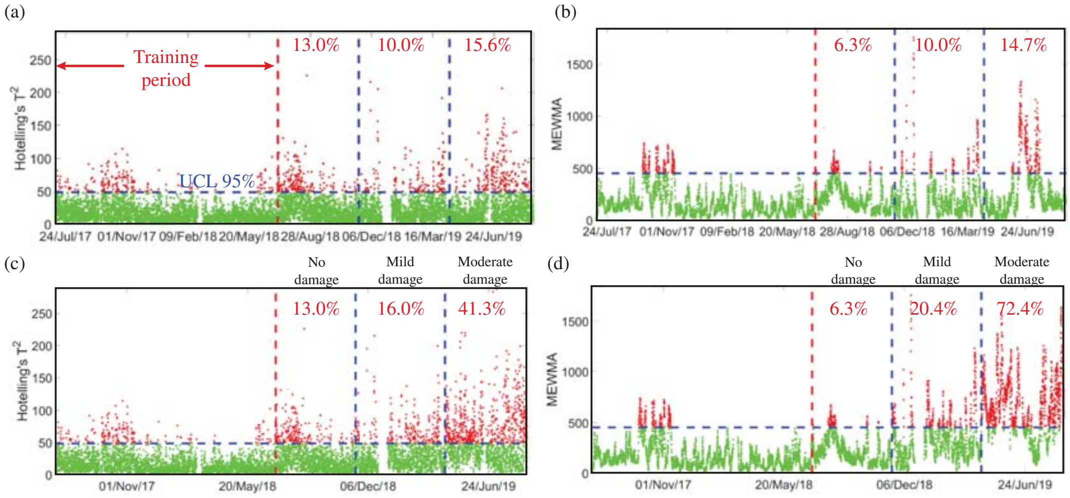

Figure 11: Control charts of the undamaged resonant frequencies of the Consoli Palace (a,b) and considering artificial damages (c,d) using the PCA regression model. The results are obtained using the Hotelling (a,c) and the MEWMA (b,d) control charts ($r = 4$).

goes from 10.0% and 14.7% to 20.4% ($\Delta Fx1 = -0.4\%$) and 72.4% ($\Delta Fx1 = -1.0\%$), that is increases of 104% and 392.517%, respectively. With regard to the results obtained using the AANN model in Fig. 12, it is observed that the number of outliers in the undamaged cases is in general larger that those obtained by the PCA model. This fact may indicate that, despite the superior capability of the AANN model to reproduce non-linear correlations, the consideration of one single cluster for non-freezing conditions may be insufficient. Furthermore, the incorporation of artificial damage in this case leads to increases of -1.89% ($\Delta Fx1 = -0.4\%$) and 219.11% ($\Delta Fx1 = -1.0\%$) in the Hotelling's control chart, and 15.33% ($\Delta Fx1 = -0.4\%$) and 184.43% ($\Delta Fx1 = -1.0\%$) in the MEWMA control chart. Note that even a decrease in the number of outliers is found in the Hotelling's control chart for a mild damage severity. Therefore, it can be concluded that this second model cannot be used to detect early-stage faults, and a larger number of clusters would be necessary to improve its efficiency.

4 CONCLUSIONS

This paper has presented a new semi-supervised two-class pattern classification method for early damage detection of structures. The proposed approach comprises five consecutive steps, including the (i) collection of data samples forming the training period; (ii) clustering analysis using the GMM method; (iii) outliers elimination using the MCD method; (iv) pattern recognition using local Principal Components Analysis; and (v) pattern classification using Hotelling and MEWMA control charts. The effectiveness of the proposed approach has been demonstrated through two different case studies, including a benchmark numerical beam structure and the Consoli Palace in Gubbio (Italy). The presented results and discussion have demonstrated the importance of outliers elimination for the correct statistical analysis of the training population and the construction of statistical models for the elimination of environmental effects. The complex relationships between the resonant frequencies and environmental temperature in the Consoli Palace have highlighted the importance of performing clustering analysis, so that local statistical models can be constructed for the different structural/environmental behaviour regimes.

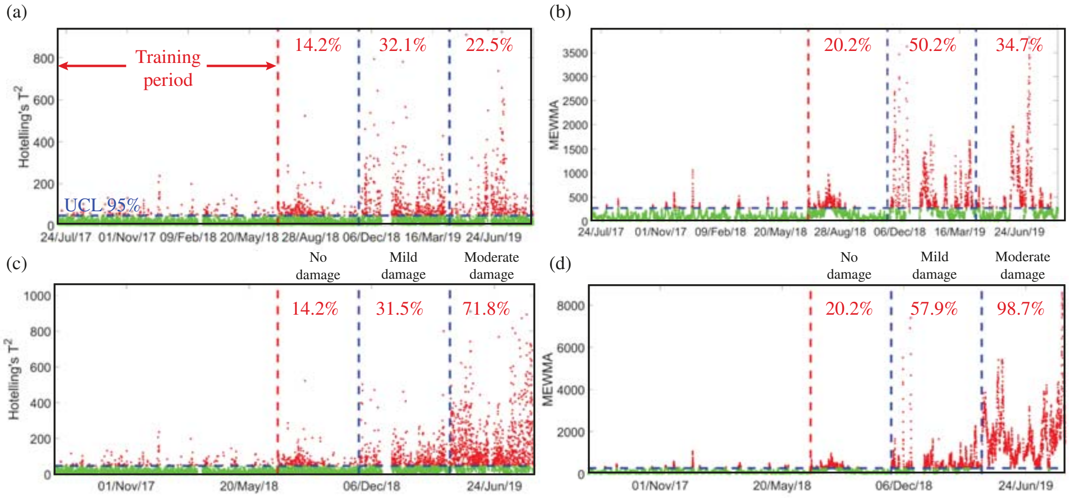

Figure 12: Control charts of the undamaged resonant frequencies of the Consoli Palace (a,b) and considering artificial damages (c,d) using the ANN regression model. The results are obtained using the Hotelling (a,c) and the MEWMA (b,d) control charts ($r = 4$).

ACKNOWLEDGEMENTS

This work was supported by the Italian Ministry of Education, University and Research (MIUR) through the funded Project of Relevant National Interest "DETECT-AGING - Degradation effects on structural safety of cultural heritage constructions through simulation and health monitoring" (protocol no. 201747Y73L).

REFERENCES

[1] C. M. Bishop. *Pattern recognition and machine learning*. springer, 2006.

[2] B. J. A. Costa, F. Magalhães, Á. Cunha, and J. Figueiras. Rehabilitation assessment of a centenary steel bridge based on modal analysis. *Engineering Structures*, 56:260–272, 2013.

[3] C. R. Farrar and K. Worden. *Structural Health Monitoring.: A Machine Learning Perspective*. John Wiley & Sons, 2012.

[4] C. Gentile, M. Guidobaldi, and A. Saisi. One-year dynamic monitoring of a historic tower: damage detection under changing environment. *Meccanica*, 51(11):2873–2889, 2016.

[5] C. Gentile, C. Poggi, A. Ruccolo, and M. Vasic. Vibration-Based Assessment of the Tensile Force in the Tie-Rods of the Milan Cathedral. *International Journal of Architectural Heritage*, pages 1–14, 2019.

[6] H. Hotteling. Multivariate quality control, illustrated by the air testing of sample bombsights. *Techniques of statistical analysis*, pages 111–184, 1947.

[7] W. H. Hu, D. H. Tang, J. Teng, S. Said, and R. Rohrmann. Structural health monitoring of a prestressed concrete bridge based on statistical pattern recognition of continuous dynamic measurements over 14 years. *Sensors*, 18(12):4117, 2018.

[8] M. Hubert, M. Debruyne, and P. J. Rousseeuw. Minimum covariance determinant and extensions. *Wiley Interdisciplinary Reviews: Computational Statistics*, 10(3):e1421, 2018.

[9] S. Ivorra, D. Foti, V. Gallo, V. Vacca, and D. Bru. Bell's dynamic interaction on a reinforced concrete bell tower. *Engineering Structures*, 183:965–975, 2019.

[10] A. Kita, N. Cavalagli, and F. Ubertini. Temperature effects on static and dynamic behavior of Consoli Palace in Gubbio, Italy. *Mechanical Systems and Signal Processing*, 120:180–202, 2019.

[11] J. Kullaa. Distinguishing between sensor fault, structural damage, and environmental or operational effects in structural health monitoring. *Mechanical Systems and Signal Processing*, 25(8):2976–2989, 2011.

[12] C. A. Lowry, W. H. Woodall, C. W. Champ, and S. E. Rigdon. A multivariate exponentially weighted moving average control chart. *Technometrics*, 34(1):46–53, 1992.

[13] F. Magalhães and Á. Cunha. Explaining operational modal analysis with data from an arch bridge. *Mechanical Systems and Signal Processing*, 25(5):1431–1450, 2011.

[14] P. Pachón, R. Castro, E. García-Macías, V. Compan, and E. Puertas. E. Torroja's bridge: Tailored experimental setup for SHM of a historical bridge with a reduced number of sensors. *Engineering Structures*, 162:11–21, 2018.

[15] L. F. Ramos, R. Aguilar, and P. B. Lourenço. Operational modal analysis of historical constructions using commercial wireless platforms. *Structural Health Monitoring*, 10(5):511–521, 2011.

[16] P. J. Rousseeuw and K. V. Driessen. A fast algorithm for the minimum covariance determinant estimator. *Technometrics*, 41(3):212–223, 1999.

[17] W. Soo Lon Wah, Y. T. Chen, G. W. Roberts, and A. Elamin. Separating damage from environmental effects affecting civil structures for near real-time damage detection. *Structural Health Monitoring*, 17(4):850–868, 2018.

[18] F. Ubertini, N. Cavalagli, A. Kita, and G. Comanducci. Assessment of a monumental masonry bell-tower after 2016 Central Italy seismic sequence by long-term SHM. *Bulletin of Earthquake Engineering*, 16(2):775–801, 2018.

[19] F. Ubertini, C. Gentile, and A. L. Materazzi. Automated modal identification in operational conditions and its application to bridges. *Engineering Structures*, 46:264–278, 2013.

[20] W. S. L. Wah, J. S. Owen, Y. T. Chen, A. Elamin, and G. W. Roberts. Removal of masking effect for damage detection of structures. *Engineering Structures*, 183:646–661, 2019.